

*Wrinkling of sandwich wide panels/beams
based on the extended high-order sandwich
panel theory: formulation, comparison with
elasticity and experiments*

**Catherine N. Phan, Nathan W. Bailey,
George A. Kardomateas & Mark
A. Battley**

Archive of Applied Mechanics

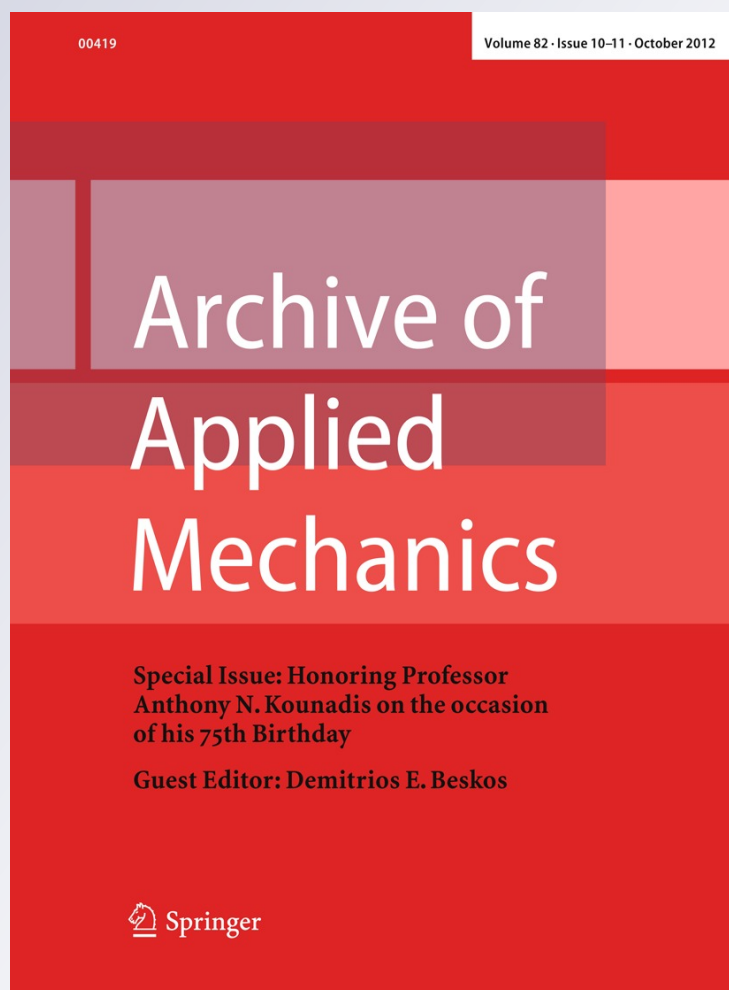
ISSN 0939-1533

Volume 82

Combined 10-11

Arch Appl Mech (2012) 82:1585-1599

DOI 10.1007/s00419-012-0673-x



Your article is protected by copyright and all rights are held exclusively by Springer-Verlag. This e-offprint is for personal use only and shall not be self-archived in electronic repositories. If you wish to self-archive your work, please use the accepted author's version for posting to your own website or your institution's repository. You may further deposit the accepted author's version on a funder's repository at a funder's request, provided it is not made publicly available until 12 months after publication.

Catherine N. Phan · Nathan W. Bailey ·
George A. Kardomateas · Mark A. Battley

Wrinkling of sandwich wide panels/beams based on the extended high-order sandwich panel theory: formulation, comparison with elasticity and experiments

Received: 18 October 2011 / Accepted: 17 February 2012 / Published online: 13 July 2012
© Springer-Verlag 2012

Abstract There exist several high-order sandwich panel theories, most notably, the first to be introduced high-order sandwich panel theory (HSAPT) assumes a constant shear stress in the core. Recently, the extended high-order sandwich panel theory (EHSAPT) was introduced, its novelty being that it allows for three generalized coordinates in the core (the axial and transverse displacements at the centroid of the core, and the rotation at the centroid of the core) instead of just one (shear stress in the core) of the earlier theory. In this paper, the EHSAPT formulation for predicting the critical wrinkling load is presented for a simply supported sandwich of general asymmetric construction. The cases of (i) applying the loading just on the face sheets with a linear core assumption and (ii) applying uniform strain loading throughout the thickness of the panel and a nonlinear core assumption are examined. The results are compared with a benchmark elasticity solution. In addition, edgewise compression experiments were conducted on glass face/Nomex honeycomb core and the ensuing wrinkling point is compared with the theoretical predictions. A comparison is also made with earlier edgewise compression experiments on aluminum face/granulated-cork core reported in literature. Other wrinkling formulas that are included in the comparison are: Hoff–Mautner and the HSAPT.

Keywords Wrinkling · Sandwich · High order · Experiments · Elasticity · Beam · Compression · Buckling

1 Introduction

Sandwich composites are a unique structural system that consists of two stiff metallic or composite thin face sheets separated by a thick core of low density. This configuration gives the sandwich material system high stiffness and strength with little resultant weight penalty. The facings carry almost all of the axial stresses and the core carries through the thickness and shear stresses. The core compressibility has an important influence in the phenomenon known as face wrinkling or local buckling. Wrinkling is a local instability phenomenon characterized by short-wave buckling of the faces as opposed to global column buckling (Euler buckling) as depicted in Fig. 1. Typically, wrinkling loads are lower than Euler Global buckling loads when the face sheets are very thin compared with the overall thickness of the panel. Wrinkling modes can be either symmetric or asymmetric as shown in Fig 1.

Several formulas can be found in literature for the critical wrinkling load. A whole chapter is devoted to these different formulas in Carlsson and Kardomateas [1]. Most notable among the simple formulas is the Hoff–Mautner formula [2] and the Allen [3] formula and the former will be used in comparing with our results.

C. N. Phan · G. A. Kardomateas (✉)
Georgia Institute of Technology, Atlanta, GA, USA
E-mail: george.kardomateas@aerospace.gatech.edu

N. W. Bailey · M. A. Battley
The University of Auckland, Auckland, New Zealand

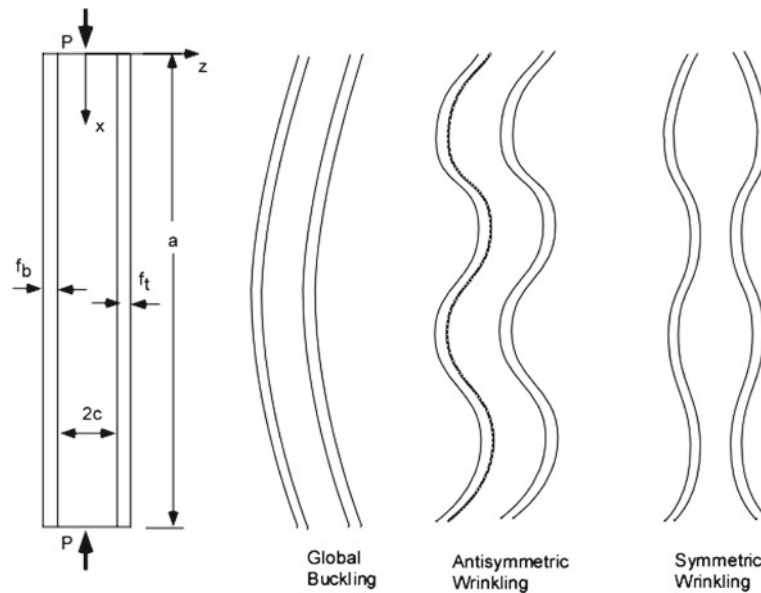


Fig. 1 Global buckling versus wrinkling

In addition, in the recent literature, several high-order theories have been presented to model the behavior of sandwich composites. The higher-order sandwich panel theory (HSAPT) [4] accounts for the transverse and shear stiffness of the core, but neglects the axial stiffness of the core and assumes a constant shear stress in the core, which is also one of the generalized coordinates of the theory. The most recent extended higher-order sandwich panel theory (EHSAPT) [5] accounts for the axial, transverse, and shear stiffness in the core and considers the rotation at the centroid of the core as one of the generalized coordinates. These theories were compared in [5] with the elasticity solution for the case of a simply supported beam undergoing a distributed sinusoidal transverse load; it was found that the EHSAPT is very close to the elasticity solution in terms of both the displacements and the transverse stress or strain, as well as axial stress through the core, and, in addition, the shear stress distributions in the core for core materials ranging from very soft to almost half the stiffness of the facesheets, unlike the HSAPT which is reasonably accurate only for very soft cores.

Another relevant study is an analytical model derived by Vonach and Rammerstorfer [6] that leads to a single explicit equation for the critical wrinkling load of sandwich plates with isotropic faces and thick orthotropic cores. The authors performed a parametric study which showed that for highly orthotropic cores (e.g., honeycombs), wrinkling depends strongly on the in-plane stiffness of the core. Their results matched numerical solutions well for very thick cores that can be assumed infinitely thick, and no interaction between the face sheets exists. This finding is important because the main difference between the recent EHSAPT and the earlier HSAPT is that the latter does not account for the in-plane stiffness of the core.

Validation of the wrinkling results from the high-order theories can be achieved by comparing with the elasticity solution for the wrinkling of a sandwich beam/wide plate, which was derived by Kardomateas [7]. In addition, validation can be achieved by comparing with experimental wrinkling loads. Historically, the success of comparisons of experimental results with analytical wrinkling models has been limited. Several semi-empirical derivations have been compared with various sandwich structure examples, however, obtaining good correlation has been hampered by inadequate testing conditions, conservative material assumptions, and manufacturing flaws [8]. Due to the sensitivity of buckling instability to the bond between the face sheet and core constituent, many aspects of material manufacturing and specimen preparation affect the variations in test results for determining the critical wrinkling stress. Wrinkling failure is a common failure mode for sandwich structures with thin face sheets and lightweight cores. During experimental tests, sandwich structures may display no or little post-wrinkling load capacity; therefore, catastrophic failure is common. Additionally, wrinkling refers to a local instability where the buckling wavelengths are typically less than the core thickness, making detection and capture of such buckling modes difficult.

In this paper, the critical wrinkling load is determined using the nonlinear differential equations of the new EHSAPT. The case study of a simply supported (S–S) sandwich beam undergoing compressive edgewise loading with symmetric geometry and same face sheet materials is used for validation with two different exper-

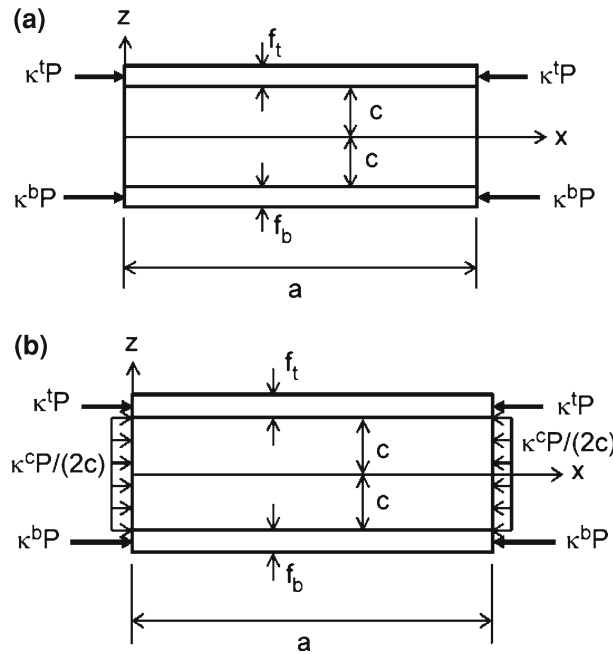


Fig. 2 The two loading cases: **a** loading on faces, linear core (PFLC); **b** uniform strain, nonlinear core (USNLC)

iments. The first set of these experiments was performed recently by the authors using a thin skin sandwich structure commonly used in interior aircraft structures, namely glass face/Nomex honeycomb core. The second set of experiments are the ones performed by Norris et al. [9] on aluminum face/granulated-cork core specimens.

In a recent study of global buckling of sandwich panels, three different solution procedures were investigated using the EHSAPT [10]: Case (a), in which the compressive loading is applied on the faces, and the core strains are assumed linear, hereby denoted as PFLC; Case (b), in which a uniform compressive strain is applied and the core strains are assumed linear, denoted by USLC; and Case (c), in which there is again a uniform compressive strain through the thickness but now the core strains are assumed nonlinear, denoted by USNLC. It was found that the EHSAPT Cases PFLC (loading on faces, linear core) and USNLC (uniform strain, nonlinear core) are nearly identical for both the soft core and moderate core configurations and both are very close to elasticity predictions, whereas Case USLC (uniform strain, linear core) diverges from elasticity to more nonconservative values for moderate cores.

The present paper begins with the EHSAPT wrinkling formulations. Two methods of solving the EHSAPT differential equations for wrinkling were undertaken, the PFLC (loading on faces, linear core) and USNLC (uniform strain, nonlinear core) as described above. The two methods were investigated to see whether the two approaches would result in different wrinkling loads. Next, the simple wrinkling formulas that will be used for comparison are described. The results from the EHSAPT are compared with these simple wrinkling formulas, as well as with the critical wrinkling loads from elasticity. Moreover, compression experiments were conducted on glass face/Nomex honeycomb core and the experimental test setup is described followed by the results and conclusions.

2 The extended high-order sandwich panel theory (EHSAPT) formulation for wrinkling

The EHSAPT [5] employs seven generalized coordinates: $u_0^t, w_0^t, u_0^c, \phi_0^c, w_0^c, u_0^b,$ and w_0^b , where the superscripts $\{t, b, c\}$ refer to the top, bottom, or core, respectively; u and w indicate the axial and transverse displacements, respectively, and ϕ denotes the rotation; moreover, the subscript 0 indicates the centroidal line (commonly the mid-line) of the respective phase.

The face sheets are assumed to be Euler-Bernoulli type beams. Referring to Fig. 2 for the definition of the geometry and the coordinate system, the top face sheet displacement field is ($c \leq z \leq c + f_t$):

$$u^t(x, z) = u_0^t(x) - \left(z - c - \frac{f_t}{2} \right) w_{0,x}^t(x), \quad (1a)$$

$$w^t(x, z) = w_0^t(x), \tag{1b}$$

and the bottom face sheet displacement field is $-(c + f_b) \leq z \leq -c$:

$$u^b(x, z) = u_0^b(x) - \left(z + c + \frac{f_b}{2} \right) w_{0,x}^b(x), \tag{1c}$$

$$w^b(x, z) = w_0^b(x). \tag{1d}$$

The core displacements $(-c \leq z \leq c)$ are as follows:

$$u^c(x, z) = z \left(1 - \frac{z^2}{c^2} \right) \phi_0^c(x) + \frac{z^2}{2c^2} \left(1 - \frac{z}{c} \right) u_0^b(x) + \left(1 - \frac{z^2}{c^2} \right) u_0^c(x) + \frac{z^2}{2c^2} \left(1 + \frac{z}{c} \right) u_0^t(x) + \frac{f_b z^2}{4c^2} \left(-1 + \frac{z}{c} \right) w_{0,x}^b(x) + \frac{f_t z^2}{4c^2} \left(1 + \frac{z}{c} \right) w_{0,x}^t(x), \tag{2a}$$

$$w^c(x, z) = \left(-\frac{z}{2c} + \frac{z^2}{2c^2} \right) w_0^b(x) + \left(1 - \frac{z^2}{c^2} \right) w_0^c(x) + \left(\frac{z}{2c} + \frac{z^2}{2c^2} \right) w_0^t(x), \tag{2b}$$

that is, the core displacements are $O(z^3)$ and $O(z^2)$ for the axial and transverse displacement fields, respectively. The displacement field of the core satisfies the displacement continuity at the top and bottom face–core interface.

Nonlinear axial strain-displacement relations for the face sheets are needed for the buckling/wrinkling formulation:

$$\epsilon_{xx}^{t,b}(x, z) = u_{,x}^{t,b}(x, z) + \frac{1}{2} \left[w_{0,x}^{t,b}(x) \right]^2. \tag{3a}$$

In the core, however, the strains are considered linear, that is, $\epsilon_{xx}^c(x, z) = u_{,x}^c(x, z)$. Later in the paper, we shall examine the effect of including nonlinear axial strains in the core, in which case the core nonlinear axial strains will be:

$$\epsilon_{xx}^c(x, z) = u_{,x}^c(x, z) + \frac{1}{2} \left[w_{,x}^c(x, z) \right]^2. \tag{3b}$$

In the following, we use the notation $1 \equiv x$, $3 \equiv z$, and $55 \equiv xz$. The constitutive relations of the face sheets are:

$$\sigma_{xx}^{t,b} = C_{11}^{t,b} \epsilon_{xx}^{t,b}, \quad \sigma_{zz}^{t,b} = C_{13}^{t,b} \epsilon_{xx}^{t,b}, \tag{4a}$$

where the stiffness constants for a beam are: $C_{11}^{t,b} = E_{11}^{t,b}$ and $C_{13}^{t,b} = \nu_{31}^{t,b} E_{11}^{t,b}$. The core constitutive properties (assuming orthotropic core) are:

$$\begin{bmatrix} \sigma_{xx}^c \\ \sigma_{zz}^c \\ \tau_{xz}^c \end{bmatrix} = \begin{bmatrix} C_{11}^c & C_{13}^c & 0 \\ C_{13}^c & C_{33}^c & 0 \\ 0 & 0 & C_{55}^c \end{bmatrix} \begin{bmatrix} \epsilon_{xx}^c \\ \epsilon_{zz}^c \\ \gamma_{xz}^c \end{bmatrix}, \tag{4b}$$

where $C_{ij}^{t,b,c}$, $ij = 11, 13, 33, 55$ are the corresponding stiffness constants.

The seven coupled nonlinear differential equations that govern the behavior of the sandwich were derived using a variational principle which considered the axial strain energy of the face sheets and the axial, transverse, and shear strain energy of the core. The derivation of the governing equations and boundary conditions follows the same pattern as for the case of global buckling and can be found in Phan et al. [10]. The following sections detail how the EHSAPT wrinkling loads are determined for two different loading approaches. The first approach (PFLC) is a simple formulation in which linear axial strains in the core are considered and loading is applied only to the face sheets. The second approach (USNLC) is a more involved formulation which takes into account nonlinear axial strains in the core and loading is applied as a uniform strain through the thickness.

2.1 Loading on the faces, linear axial strain in the core (PFLC)

In this approach, concentrated compressive loads (per unit width) $\kappa^t P$ and $\kappa^b P$ are applied on the top and bottom facesheets, respectively, such that they sum up to the total applied load P , and the prebuckled axial strains $\epsilon_{xxp}^i = a_{11}^i \sigma_{xxp}^i$ for $i = t, b$ are equal on the top and bottom faces (Fig. 2a). Imposing these conditions leads to:

$$\kappa^t = \frac{a_{11}^b f_t}{a_{11}^t f_b + a_{11}^b f_t}, \quad \kappa^b = \frac{a_{11}^t f_b}{a_{11}^t f_b + a_{11}^b f_t}. \tag{5a}$$

The critical load for an asymmetric geometry and material configuration can be determined using the perturbation approach:

$$N^i(x) = N_p^i(x) + \xi N_s^i(x) \quad (i = t, b, c), \tag{5b}$$

$$u_0^i(x) = u_p(x) + \xi u_{0s}^i(x) \quad (i = t, b), \tag{5c}$$

$$w_0^i(x) = \xi w_{0s}^i(x), \quad M^i(x) = \xi M_s^i(x), \quad (i = t, b, c), \tag{5d}$$

$$u_0^c(x) = \xi u_{0s}^c(x), \quad \phi_0^c(x) = \xi \phi_{0s}^c(x), \quad V^c(x) = \xi V_s^c(x). \tag{5e}$$

where N^i is the axial stress resultant (per unit width), M^i is the moment stress resultant (per unit width), and V^i is the shear stress resultant (per unit width) for $i = t, b$, or c . The subscript p stands for the primary (prebuckled) state, while the subscript s stands for the secondary (perturbed) state, and ξ is an infinitesimally small quantity. In the PFLC approach, $N_p^i(x) = -\kappa^i P$ ($i = t, b$), where the negative sign is introduced because positive N is tensile and the applied load is compressive.

The wrinkling mode n for the simply supported beam is in the form:

$$u_{0s}^{t,b,c} = U_{0n}^{t,b,c} \cos \frac{n\pi x}{a}, \quad \phi_{0s}^c = \Phi_{0n}^c \cos \frac{n\pi x}{a}, \quad w_{0s}^{t,b,c} = W_{0n}^{t,b,c} \sin \frac{n\pi x}{a}. \tag{6}$$

The perturbation assumption with the assumed modes leads to seven algebraic equations that contain the loading per unit width P (the eigenvalue to be solved for), and these are: for the top face two equations:

$$\begin{aligned} &U_0^b \left(-\frac{7}{30c} C_{55}^c + \frac{cn^2\pi^2}{35a^2} C_{11}^c \right) + U_{0n}^c \left(-\frac{4}{3c} C_{55}^c + \frac{2cn^2\pi^2}{15a^2} C_{11}^c \right) \\ &+ \Phi_0^c \left(-\frac{4}{5} C_{55}^c + \frac{2c^2n^2\pi^2}{35a^2} C_{11}^c \right) + U_0^t \left(\frac{47}{30c} C_{55}^c + \frac{6cn^2\pi^2}{35a^2} C_{11}^c + \frac{f_t n^2 \pi^2}{a^2} C_{11}^t \right) \\ &+ W_0^b \left(-\frac{cf_b n^3 \pi^3}{70a^3} C_{11}^c - \eta_2^b \frac{n\pi}{a} \right) + W_0^c \frac{n\pi \beta_1}{a} + W_0^t \left(\frac{3cf_t n^3 \pi^3}{35a^3} C_{11}^c + \eta_3^t \frac{n\pi}{a} \right) = 0 \end{aligned} \tag{7a}$$

$$\begin{aligned} &U_0^b \left(\frac{cf_t n^3 \pi^3}{70a^3} C_{11}^c + \eta_2^t \frac{n\pi}{a} \right) + U_0^c \left(\frac{cf_t n^3 \pi^3}{15a^3} C_{11}^c - \eta_6^c \frac{n\pi}{a} \right) + \Phi_0^c \left(\frac{c^2 f_t n^3 \pi^3}{35a^3} C_{11}^c - \eta_4^t \frac{n\pi}{a} \right) \\ &+ U_0^t \left(\frac{3cf_t n^3 \pi^3}{35a^3} C_{11}^c + \frac{n\pi}{a} \eta_3^t \right) + W_0^b \left(\frac{C_{33}^c}{6c} - \frac{cf_b f_t n^4 \pi^4}{140a^4} C_{11}^c - \beta_2 \frac{n^2 \pi^2}{a^2} \right) + W_0^c \left(-\frac{4}{3c} C_{33}^c - \eta_7^t \frac{n^2 \pi^2}{a^2} \right) \\ &+ W_0^t \left(-\kappa^t P \frac{n^2 \pi^2}{a^2} + \frac{7}{6c} C_{33}^c + \frac{3cf_t^2 n^4 \pi^4}{70a^4} C_{11}^c + \frac{f_t^3 n^4 \pi^4}{12a^4} C_{11}^t - \eta_8^t \frac{n^2 \pi^2}{a^2} \right) = 0 \end{aligned} \tag{7b}$$

for the core three equations:

$$\begin{aligned} &U_0^b \left(-\frac{4}{3c} C_{55}^c + \frac{2cn^2\pi^2}{15a^2} C_{11}^c \right) + U_0^c \left(\frac{8}{3c} C_{55}^c + \frac{16cn^2\pi^2}{15a^2} C_{11}^c \right) + U_0^t \left(-\frac{4}{3c} C_{55}^c + \frac{2cn^2\pi^2}{15a^2} C_{11}^c \right) \\ &+ W_0^b \left(\frac{\eta_6^b n\pi}{a} - \frac{cf_b n^3 \pi^3}{15a^3} C_{11}^c \right) + W_0^t \left(\frac{cf_t n^3 \pi^3}{15a^3} C_{11}^c - \frac{\eta_6^t n\pi}{a} \right) = 0 \end{aligned} \tag{7c}$$

$$U_0^b \left(\frac{4}{5} C_{55}^c - \frac{2c^2 n^2 \pi^2}{35a^2} C_{11}^c \right) + \Phi_0^c \left(\frac{8c}{5} C_{55}^c + \frac{16c^3 n^2 \pi^2}{105a^2} C_{11}^c \right) + U_0^t \left(-\frac{4}{5} C_{55}^c + \frac{2c^2 n^2 \pi^2}{35a^2} C_{11}^c \right)$$

$$+ W_0^b \left(\frac{c^2 f_b n^3 \pi^3}{35a^3} C_{11}^c - \frac{\eta_4^b n \pi}{a} \right) + W_{0n}^c \left(\frac{4c\beta_1 n \pi}{3a} \right) + W_0^t \left(\frac{c^2 f_t n^3 \pi^3}{35a^3} C_{11}^c - \frac{\eta_4^t n \pi}{a} \right) = 0 \quad (7d)$$

$$- U_0^b \left(\frac{\beta_1 n \pi}{a} \right) + \Phi_0^c \left(\frac{4c\beta_1 n \pi}{3a} \right) + U_0^t \left(\frac{\beta_1 n \pi}{a} \right) - W_0^b \left(\frac{4}{3c} C_{33}^c + \frac{\eta_7^i n^2 \pi^2}{a^2} \right) + W_0^c \left(\frac{8}{3c} C_{33}^c + \frac{16cn^2 \pi^2}{15a^2} C_{55}^c \right) - W_0^t \left(\frac{4}{3c} C_{33}^c + \frac{\eta_7^i n^2 \pi^2}{a^2} \right) = 0 \quad (7e)$$

and for the bottom face two equations as follows:

$$U_0^b \left(\frac{47}{30c} C_{55}^c + \frac{6cn^2 \pi^2}{35a^2} C_{11}^c + f_b \frac{n^2 \pi^2}{a^2} C_{11}^b \right) + U_0^c \left(-\frac{4}{3c} C_{55}^c + \frac{2cn^2 \pi^2}{15a^2} C_{11}^c \right) + \Phi_0^c \left(\frac{4}{5} C_{55}^c - \frac{2c^2 n^2 \pi^2}{35a^2} C_{11}^c \right) + U_0^t \left(-\frac{7}{30c} C_{55}^c + \frac{cn^2 \pi^2}{35a^2} C_{11}^c \right) + W_0^b \left(-\frac{3cf_b n^3 \pi^3}{35a^3} C_{11}^c - \eta_3^b \frac{n \pi}{a} \right) - W_0^c \left(\frac{n \pi}{a} \beta_1 \right) + W_0^t \left(\frac{cf_t n^3 \pi^3}{70a^3} C_{11}^c + \eta_2^t \frac{n \pi}{a} \right) = 0 \quad (7f)$$

$$U_0^b \left(-\frac{3cf_b n^3 \pi^3}{35a^3} C_{11}^c - \eta_3^b \frac{n \pi}{a} \right) + U_0^c \left(-\frac{cf_b n^3 \pi^3}{15a^3} C_{11}^c - \eta_6^b \frac{n \pi}{a} \right) + \Phi_{0n}^c \left(\frac{c^2 f_b n^3 \pi^3}{35a^3} C_{11}^c - \eta_4^b \frac{n \pi}{a} \right) + U_0^t \left(-\frac{cf_b n^3 \pi^3}{70a^3} C_{11}^c - \eta_2^b \frac{n \pi}{a} \right) + W_0^b \left(-\kappa^b P \frac{n^2 \pi^2}{a^2} + \frac{7}{6c} C_{33}^c + \frac{3cf_b^2 n^4 \pi^4}{70a^4} C_{11}^c + \frac{f_b^3 n^4 \pi^4}{12a^4} C_{11}^b - \eta_8^b \frac{n^2 \pi^2}{a^2} \right) + W_0^c \left(-\frac{4}{3c} C_{33}^c - \eta_7^b \frac{n^2 \pi^2}{a^2} \right) + W_0^t \left(\frac{C_{33}^c}{6c} - \frac{cf_b f_t n^4 \pi^4}{140a^4} C_{11}^c - \beta_2 \frac{n^2 \pi^2}{a^2} \right) = 0 \quad (7g)$$

These can be cast in the following matrix form:

$$\{[K_{LC}] - \frac{n^2 \pi^2}{a^2} [G_a][I]\} \{U\} = \{0\}. \quad (7h)$$

where $[K_{LC}]$ is a 7×7 matrix involving material stiffnesses and sandwich dimensions, and each element is given in Appendix A. The subscript LC is used to denote that the sandwich system has linear strains in the core. Later in the paper another matrix, the K_{NLC} will represent additional terms that account for nonlinear axial strains in the core. The loading vector is represented by $[G_a] = [0, 0, 0, 0, \kappa^b P, 0, \kappa^t P]$. Seven unknown displacement amplitudes make up the vector $\{U\} = [U_0^b, U_0^c, \Phi_0^c, U_0^t, W_0^b, W_0^c, W_0^t]^T$. The critical load is determined by finding the value of P for which the system has a nontrivial solution or finding P by zeroing the determinant:

$$\det\{[K_{LC}] - \frac{n^2 \pi^2}{a^2} [G_a][I]\} = 0. \quad (7i)$$

2.2 Uniform strain loading, nonlinear axial strain in the core (USNLC)

In this case (Fig. 2b), the top and bottom phases are compressively loaded with concentrated loads (per unit width) $\kappa^t P$ and $\kappa^b P$, respectively, and the core is loaded with a compressive uniformly distributed load (per unit width) $\kappa^c \frac{P}{2c}$, such that they sum up to the total applied load P , and each phase has the same axial strain $\epsilon_{x xp}^i = a_{11}^i \sigma_{x xp}^i$ for $i = t, b, c$. Imposing these conditions leads to:

$$\kappa^t = \frac{a_{11}^b a_{11}^c f_t}{a_{11}^b a_{11}^t 2c + a_{11}^b a_{11}^c f_t + a_{11}^t a_{11}^c f_b}, \quad (8a)$$

$$\kappa^b = \frac{a_{11}^t a_{11}^c f_b}{a_{11}^b a_{11}^t 2c + a_{11}^b a_{11}^c f_t + a_{11}^t a_{11}^c f_b}, \quad (8b)$$

$$\kappa^c = \frac{a_{11}^t a_{11}^b 2c}{a_{11}^b a_{11}^t 2c + a_{11}^b a_{11}^c f_t + a_{11}^t a_{11}^c f_b}. \quad (8c)$$

When a uniform strain exists in the core, the face sheets have a nonzero transverse displacement at the primary state, which is due to the Poisson's effect on the core during compression (as opposed to the previous case). Thus, the top and bottom face sheets have primary state transverse displacements that are equal, yet opposite in direction, that is, w_p and $-w_p$, respectively; furthermore, they are constant along x . Moreover, when the loading is uniform strain, the axial displacement at the primary state in each phase is the same, denoted by u_p . Therefore, in this case, the displacements in the perturbation approach are:

$$u_0^i(x) = u_p(x) + \xi u_{0s}^i(x) \quad (i = t, b, c), \quad (9a)$$

$$\phi_0^c(x) = \xi \phi_{0s}^c(x), \quad (9b)$$

$$w_0^t(x) = w_p + \xi w_{0s}^t(x), \quad (9c)$$

$$w_0^c(x) = \xi w_{0s}^c(x), \quad (9d)$$

$$w_0^b(x) = -w_p + \xi w_{0s}^b(x). \quad (9e)$$

In the study of global buckling using EHSAPT in Phan et al. [10], it was shown that when loading on the core exists, nonlinear axial strain in the core needs to be considered. In fact, it was shown that neglecting nonlinear axial strains in this case would lead to inaccurate and nonconservative results. Linear axial strains in the core are acceptable in the PFLC case because the core is not loaded in that case.

The resulting wrinkled state equations in matrix form are:

$$[K_{LC}] + [K_{NLC}] - \frac{n^2 \pi^2}{a^2} [G_c][I]\{U\} = \{0\}, \quad (10a)$$

where $[K_{LC}]$ is the same as in the PFLC approach, and $[K_{NLC}]$ contains the additional terms that account for nonlinear axial strains in the core:

$$K_{NLC} = \frac{n^2 \pi^2}{a^2} (c C_{11}^c u_{p,x} + C_{13}^c w_p) \begin{bmatrix} 0 & 0 & 0 & 0 & 0 & 0 \\ 0 & 0 & 0 & 0 & 0 & 0 \\ 0 & 0 & 0 & 0 & 0 & 0 \\ 0 & 0 & 0 & 0 & 0 & 0 \\ 0 & 0 & 0 & \frac{4}{15} & \frac{2}{15} & -\frac{1}{15} \\ 0 & 0 & 0 & \frac{2}{15} & -\frac{14}{15} & \frac{2}{15} \\ 0 & 0 & 0 & -\frac{1}{15} & \frac{2}{15} & \frac{4}{15} \end{bmatrix}. \quad (10b)$$

Note that $[K_{NLC}]$ depends on the primary state displacements, in particular, on $u_{p,x}$, (the x -derivative of the uniform axial displacement) and w_p (the uniform transverse displacement of the top face sheet due to the Poisson's effect in the axially loaded core). The solution to the primary state displacements can be obtained by solving the prebuckled-state equations and are:

$$u_p = -\frac{a_{11}^t \kappa^t P}{f_t} x = -\frac{a_{11}^b \kappa^b P}{f_b} x = -\frac{a_{11}^c \kappa^c P}{2c} x; \quad w_p = -\frac{c C_{13}^c}{C_{33}^c} u_{p,x}. \quad (10c)$$

We should note that the solution procedure for this case becomes more complicated because both primary and secondary generalized coordinates appear in the wrinkled state set of equations. For the case of global buckling in [10], the extra work required to solve both sets of equations did not make significant gains in accuracy compared with the PFLC approach.

Now that the nonlinear axial strain of the core is considered, the resultant load on each phase appears in the force vector:

$$G_c = [0, 0, 0, 0, \kappa^t P, \kappa^c P, \kappa^b P]^t. \quad (10d)$$

Again, the critical load is determined by solving the value of P which gives a nontrivial solution to the buckled state equations, that is, by zeroing the determinant:

$$\det\{[K_{LC}] + [K_{NLC}] - \frac{n^2 \pi^2}{a^2} [G_c][I]\} = 0. \quad (10e)$$

3 Critical wrinkling load from the HSAPT and other wrinkling formulas

An earlier high-order theory for sandwich panels is the HSAPT, which assumes constant shear in the core and accounts for the transverse and shear stiffness of the core, but assumes that the axial stress in the core is negligible [4]. The wrinkling formulas from HSAPT are derived in [11].

In the case of a symmetrical construction in which the two skins are identical, the symmetric wrinkling critical load per unit width from the HSAPT is:

$$P_{cr,HSAPT,symm} = \frac{2[E_{33}^c + c(EI)\alpha_n^4]}{c\alpha_n^2}, \quad (11a)$$

where

$$EI = E_{11}^f f^3 / 12; \quad \alpha_n = n\pi/a. \quad (11b)$$

In the case of antisymmetric wrinkling, the critical load from the HSAPT is:

$$P_{cr,HSAPT,antisymm} = P_e \left\{ \frac{1 + \left[1 + \frac{(2c)^2 G_{31}^c n^2 \pi^2}{12 E_3^c a^2} \right] \left(\frac{P_{ef}}{P_c} - \frac{P_{ef}^2}{P_c P_e} \right)}{1 + \left[1 + \frac{(2c)^2 G_{31}^c n^2 \pi^2}{12 E_3^c a^2} \right] \frac{(P_e - P_{ef})}{P_c}} \right\}, \quad (12a)$$

where

$$P_e = E_{11}^f \frac{n^2 \pi^2}{a^2} \left[\frac{f^3}{6} + \frac{f(2c + f)^2}{2} \right], \quad (12b)$$

$$P_{ef} = E_{11}^f \frac{n^2 \pi^2}{a^2} \frac{f^3}{6}; \quad P_c = G_{c31} \frac{(2c + f)^2}{2c}, \quad (12c)$$

Among the other simple wrinkling formulas, which are outlined in Carlsson and Kardomateas [1], Hoff and Mautner's formula is mostly known and used in the form:

$$\sigma_{cr,HoffMautner} = 0.5(E_{11}^f E_{33}^c G_{31}^c)^{(1/3)}, \quad (13a)$$

where the critical stress refers to the face sheets. The cubic root form of the Hoff–Mautner equation was derived using an energy approach for the problem of symmetric wrinkling of a sandwich (with isotropic material and negligible axial rigidity in the core). The theoretical approach led to a coefficient of 0.91 in front of the cubic root of the Hoff–Mautner formulation ([2]). However, a conservative version of the formula with a coefficient of 0.5 instead of 0.91 is commonly used. The formula is independent of the sandwich geometry and mode of wrinkling and has been used as a wrinkling failure approximation for sandwich design. As can be seen in Hoff–Mautner's simple formula, the transverse stiffness of the core in particular is critical in improving the susceptibility of a sandwich material to wrinkling failure. For the case of uniform strain loading on a sandwich with a symmetric configuration, the Hoff–Mautner critical load can also be expressed as $P_{cr,HoffMautner} = \sigma_{cr,HoffMautner}(2fb)$, that is, the entire load is assumed to be carried by the face sheets.

4 Comparison of theories with elasticity

An elasticity solution to the wrinkling phenomenon of a simply supported sandwich beam was presented by Kardomateas [7]. This elasticity solution can serve as a benchmark to determine the accuracy of the different sandwich panel theories and simple wrinkling formulas. Tables 1 through 4 give the critical loads (normalized with the Euler load) for sandwich beams with length ratio $a/h_{tot} = 5$ and varying thickness ratios f/h_{tot} , where $h_{tot} = 2(f + c)$ is the total beam thickness. The four tables correspond to the following material configurations: Isotropic face and core with $E_f/E_c = 1,000$, Isotropic face and core with $E_f/E_c = 500$, E-glass/polyester faces with PVC/R75 foam core, and graphite/epoxy faces with glass/phenolic honeycomb core, respectively. These tables compare the elasticity results to the wrinkling predictions from the two methods of EHSAPT (PFLC and USNLC), the HSAPT, and the Hoff–Mautner (semi-empirical constant = 0.5). The tables also show the mode and percent Error with respect to elasticity.

Table 1 Critical loads for $E_f/E_c = 1,000$; normalized with the Euler load (w/o shear)

f/h_{tot}	Elasticity (n)	Hoff (n) (Error %)	HSAPT (n) (Error %)	EHSAPT ^a (n) (Error %)	EHSAPT ^b (n) (Error %)
0.01	0.07381 (A24)	0.04038 (27) (-45.3 %)	0.02654 (S20) (-64.0 %)	0.07909 (A22) (+7.2 %)	0.08228 (A22) (+11.5 %)
0.02	0.07393 (A12)	0.04154 (13) (-43.8 %)	0.03902 (S12) (-47.2 %)	0.07080 (A12) (-4.2 %)	0.07212 (A12) (-2.5 %)
0.03	0.07288 (A7)	0.04251 (9) (-41.7 %)	0.04945 (S9) (-32.2 %)	0.06967 (A8) (-4.4 %)	0.07040 (A8) (-3.4 %)
0.04	0.06489 (A1)	0.04345 (7) (-33.0 %)	0.05900 (S7) (-9.1 %)	0.06389 (A1) (-1.5 %)	0.06391 (A1) (-1.5 %)
0.05	0.05411 (A1)	0.04439 (5) (-18.0 %)	0.05336 (A1) (-1.4 %)	0.05336 (A1) (-1.4 %)	0.05337 (A1) (-1.4 %)

Superscripts a and b are for method PFLC and USNLC, respectively. A and S in the wave numbers stand for anti-symmetric and symmetric, respectively

Table 2 Critical loads for $E_f/E_c = 500$; normalized with the Euler load (w/o shear)

f/h_{tot}	Elasticity (n)	Hoff (n) (Error %)	HSAPT (n) (Error %)	EHSAPT ^a (n) (Error %)	EHSAPT ^b (n) (Error %)
0.01	0.1222 (A30)	0.0631 (34) (-48.4 %)	0.0370 (S24) (-69.8 %)	0.1370 (A26) (+12.1 %)	0.1479 (A26) (+21.1 %)
0.02	0.1210 (A15)	0.0654 (17) (-45.9 %)	0.0548 (S14) (-54.7 %)	0.1162 (A15) (-4.0 %)	0.1207 (A15) (-0.3 %)
0.03	0.1211 (A10)	0.0672 (11) (-44.5 %)	0.0698 (S11) (-42.3 %)	0.1143 (A10) (-5.6 %)	0.1169 (A10) (-3.4 %)
0.04	0.1188 (A6)	0.0687 (9) (-42.1 %)	0.0836 (S9) (-29.6 %)	0.1128 (A7) (-5.0 %)	0.1144 (A7) (-3.7 %)
0.05	0.1027 (A1)	0.0703 (7) (-31.6 %)	0.0962 (S7) (-6.3 %)	0.1003 (A1) (-2.3 %)	0.1003 (A1) (-2.3 %)

Superscripts a and b are for method PFLC and USNLC, respectively. A and S in the wave numbers stand for anti-symmetric and symmetric, respectively

For Tables 1 and 2, results are produced for the following configuration: isotropic faces and core with $E_f/E_c = 1,000$ and 500 , $\nu_f = 0.35$ and $\nu_c = 0$. Table 3 gives results for E-glass/polyester unidirectional facings and R75 cross-linked PVC foam core with the facings moduli (in GPa): $E_1^f = 40$, $E_2^f = E_3^f = 10$, $G_{23}^f = 3.5$, $G_{12}^f = G_{31}^f = 4.5$; and the facings Poisson's ratios: $\nu_{12}^f = 0.26$, $\nu_{23}^f = 0.40$, $\nu_{31}^f = 0.065$. The PVC core is isotropic with modulus $E^c = 0.075$ GPa and Poisson's ratio $\nu^c = 0.3$. The axial modulus ratio of the facings and the core is close to 500. In general, we can make the following conclusions for the isotropic core case:

- (1) Sandwich structures will exhibit local wrinkling as f/h_{tot} becomes small (i.e., sandwiches with relatively thin faces), and global buckling as f/h_{tot} becomes bigger (i.e., sandwiches with relatively thick faces).
- (2) The semi-empirical Hoff–Mautner formula is always very conservative between 18 and 50% under that of elasticity.
- (3) The HSAPT is inaccurate in predicting wrinkling loads for sandwiches with very thin faces, underpredicting the critical load by as much as 70% for the more moderately stiffer core configuration with $E_f/E_c = 500$ and $f/h_{tot} = 0.01$.

Table 3 Critical loads for E-glass/polyester faces and PVC/R75 foam core; normalized with the Euler load (w/o shear)

f/h_{tot}	Elasticity (n)	Hoff (n) (Error %)	HSAPT (n) (Error %)	EHSAPT ^a (n) (Error %)	EHSAPT ^b (n) (Error %)
0.01	0.10230 (A30)	0.05549 (32) (-45.8 %)	0.03586 (S23) (-65.0 %)	0.10775 (A25) (+5.3 %)	0.11583 (A25) (+13.2 %)
0.02	0.10120 (A15)	0.05749 (16) (-43.2 %)	0.05307 (S14) (-47.6 %)	0.09593 (A14) (-5.2 %)	0.09932 (A14) (-1.9 %)
0.03	0.10080 (A9)	0.05898 (11) (-41.5 %)	0.06751 (S10) (-33.0 %)	0.09533 (A9) (-5.4 %)	0.09720 (A9) (-3.6 %)
0.04	0.09096 (A1)	0.06035 (8) (-33.6 %)	0.08080 (S8) (-11.2 %)	0.08953 (A1) (-1.6 %)	0.08957 (A1) (-1.5 %)
0.05	0.07596 (A1)	0.06170 (6) (-18.8 %)	0.07486 (A1) (-1.4 %)	0.07495 (A1) (-1.3 %)	0.07497 (A1) (-1.3 %)

Superscripts a and b are for method PFLC and USNLC, respectively. A and S in the wave numbers stand for anti-symmetric and symmetric, respectively

Table 4 Critical loads for graphite/epoxy faces and glass/phenolic honeycomb core; normalized with the Euler load (w/o shear)

f/h_{tot}	Elasticity (n)	Hoff (n) (Error %)	HSAPT (n) (Error %)	EHSAPT ^a (n) (Error %)	EHSAPT ^b (n) (Error %)
0.01	0.07037 (A26)	0.04277 (15) (-39.2 %)	0.03947 (S24) (-43.9 %)	0.07099 (A25) (+0.9 %)	0.07147 (A25) (+1.6 %)
0.02	0.06552 (A1)	0.04371 (7) (-33.3 %)	0.05773 (S14) (-11.9 %)	0.06506 (A9) (-0.7 %)	0.06517 (A9) (-0.5 %)
0.03	0.04576 (A1)	0.04463 (5) (-2.5 %)	0.04558 (A1) (-0.4 %)	0.04559 (A1) (-0.4 %)	0.04559 (A1) (-0.4 %)
0.04	0.03577 (A1)	0.04556 (4) (+27.4 %)	0.03564 (A1) (-0.4 %)	0.03564 (A1) (-0.4 %)	0.03564 (A1) (-0.4 %)
0.05	0.02988 (A1)	0.04652 (3) (+55.7 %)	0.02978 (A1) (-0.3 %)	0.02978 (A1) (-0.3 %)	0.02978 (A1) (-0.3 %)

Superscripts a and b are for method PFLC and USNLC, respectively. A and S in the wave numbers stand for anti-symmetric and symmetric, respectively

- (4) The EHSAPT is the most accurate with the USNLC approach (uniform strain, nonlinear core) predicting slightly higher critical loads than the PFLC approach (loading on faces, linear core). In general, USNLC is more accurate than the PFLC when the beam wrinkles for all f/h_{tot} other than 0.01. The deviation from elasticity for the USNLC is no more than about 4%.
- (5) The EHSAPT PFLC approach has good accuracy for the range of thickness ratios with at most 12% Error for the extreme case of $f/h_{tot} = 0.01$ for isotropic face and core with $E_f/E_c = 500$ (Table 2).
- (6) The HSAPT predicts symmetric wrinkling modes, while the EHSAPT predicts antisymmetric wrinkling modes, similar to elasticity.

Table 4 gives results for graphite/epoxy unidirectional facings and hexagonal glass/phenolic honeycomb core with the facings moduli (in GPa): $E_1^f = 181$, $E_2^f = E_3^f = 10.3$, $G_{23}^f = 5.96$, $G_{12}^f = G_{31}^f = 7.17$; and the facings Poisson's ratios: $\nu_{12}^f = 0.28$, $\nu_{23}^f = 0.49$, $\nu_{31}^f = 0.0159$. The honeycomb core moduli are in (GPa): $E_1^c = E_2^c = 0.032$, $E_3^c = 0.390$, $G_{23}^c = G_{31}^c = 0.048$, $G_{12}^c = 0.013$; and the core Poisson's ratio $\nu_{31}^c = \nu_{32}^c = \nu_{21}^c = 0.25$. For this orthotropic core case, the following observations are made:

- (7) According to elasticity, the beam wrinkles only at $f/h_{tot} = 0.01$ and globally buckles for the relatively thicker faces.

- (8) The semi-empirical Hoff–Mautner formula is always very conservative with respect to elasticity when the beam wrinkles, but can be nonconservative when the beam globally buckles (it would not be expected to be applicable for global buckling, anyway).
- (9) The HSAPT is very conservative when the beam wrinkles, but becomes more accurate for thicker faces.
- (10) The EHSAPT (both PFLC and USNLC approaches) is very accurate even at the extreme case of $f/h_{\text{tot}} = 0.01$.

The wrinkling results display some trends that were seen when studying the global buckling phenomenon in Phan et al. [10], such as that the HSAPT tends to become less accurate and underpredicts critical loads for very thin faces and that both the HSAPT and the EHSAPT (PFLC and USNLC) converge for thicker faces (bigger f/h_{tot}). The discrepancy between HSAPT and EHSAPT for very low f/h_{tot} (when the beam is most susceptible to wrinkling), but convergence for higher f/h_{tot} (when the beam tends to globally buckle), indicates that including the axial rigidity of the core is important during wrinkling. Though both high-order theories have the same order of displacements in z in the core, the theories differ in shear stress distribution through the core. The HSAPT ignores the axial rigidity of the core, which makes the shear stress through the thickness constant. The EHSAPT accounts for the axial rigidity in the core and the shear stress is parabolic. In Kardomateas [7], the most accurate formula for wrinkling of isotropic faces and cores was that of Goodier and Neou [12], which accounts for the compressive axial stress in the core. However the Goodier and Neou formula no longer exhibited good accuracy when the phases were orthotropic. The EHSAPT, however, can show good accuracy in these cases.

5 Experimental study

Sandwich construction consisting of a Nomex honeycomb core with a glass fiber and phenolic resin facesheet is common in aerospace applications. The material for this study is a panel consisting of 0.5-mm-thick glass-phenolic facesheets (L528-7781) and a 24.4-mm Nomex honeycomb core (HRH 10-3.0). Sandwich panels were manufactured using layers of honeycomb core, adhesive and pre-impregnated face sheets, which are consolidated in a heated press. Due to the nature of honeycomb, the core properties are anisotropic with a large transverse stiffness compared with the in-plane properties. The stiffer ribbon direction of the core was aligned with the loading or compression direction for all tests. Specimen geometry is shown in Figure 3 and illustrates the area of core removed and replaced with epoxy resin. This region of potting was required to prevent edge failure of the structure during loading whereby the face sheet delaminates from the core at the boundary due to the contact with the loading platen at this point. Premature edge failure occurs at a significantly lower load than the anticipated failure mode of skin wrinkling. After the edges were potted, they were post-machined to ensure the ends were parallel and square. The data for the materials used are in Table 5.

The residual strength testing was carried out using an edgewise compression test method ASTM C364-07. The test fixture shown in Figure 3 was made of two identical loading plates with bars to lightly clamp the specimen to assist in preventing end failures. A spherical head was used to evenly distribute the load over the top plate. The load was applied at a displacement rate of 0.5 mm/min and wrinkling failure occurred within 3–6 min.

Seven specimens were instrumented with strain gauges to measure longitudinal or compressive strain in the center of the face sheets during edgewise loading. The purpose of the direct strain measurement was to ensure even distribution of the load between the face sheets. Strain was recorded to the data acquisition program in real-time. Prior to testing, a 50 N compressive preload was applied and the strain in each face sheet was measured. The spherical head was then adjusted until the strain distribution between the face sheets was within 5%. This preload ensured that a more even loading distribution of the face sheets was achieved. Without this preloading alignment, and adjustment of the spherical head, the average critical load reduced by 12%.

Table 6 shows the measured critical loads P for the 7 specimens tested. The average compressive critical load was 17.8 kN with a standard deviation of 0.646 kN. The onset of wrinkling failure was catastrophic. The specimens were examined after failure and the face sheets were observed to have failed between the loading platens with a crack propagating from one edge of the specimen. It is believed that wrinkling was the cause of failure and not face crushing because the compressive stress in the face at the time of failure was 22% below the yield strength of the virgin face sheet material. The variation in critical load was also very good with only a 3.6% coefficient of variation from the seven tests (attributed to the careful alignment of the loading platens via strain measurement). Though the variation in critical load among the seven specimens was small, scatter in

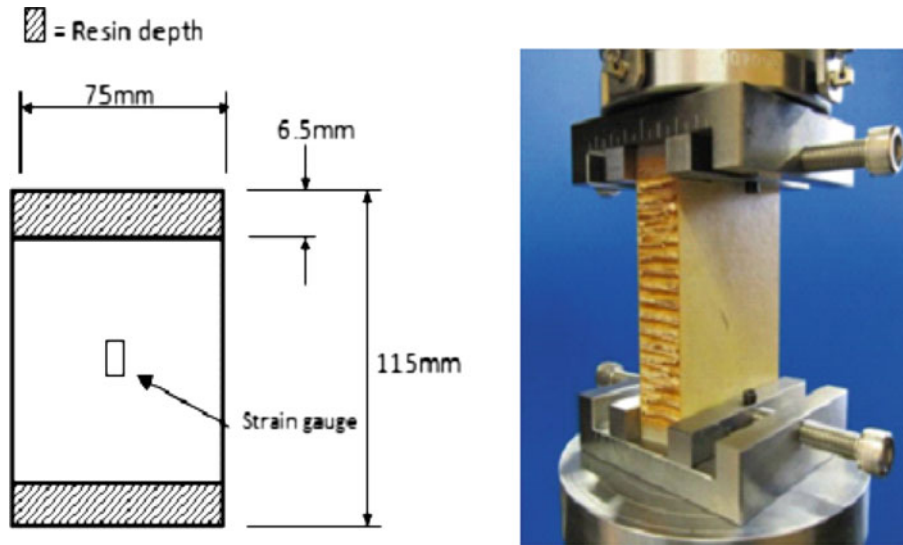


Fig. 3 Details of the test setup

Table 5 Material and geometry data for glass-phenolic facesheet and Nomex honeycomb core sandwich

	Facesheet glass-phenolic	Core Nomex honeycomb 1/8-3.0
Thickness, mm	0.5	24.4
Width, mm	75	75
Length, mm	115	115
E_1 , MPa	22,000	0.44
E_2 , MPa	22,000	0.29
E_3 , MPa	–	138
G_{13} , MPa	–	40
G_{23} , MPa	–	25
ν_{13}	–	0.01
ν_{31}	–	3.136
Longitudinal tensile strength σ_1 , MPa	300	–
In-plane transverse tensile strength σ_2 , MPa	300	–
Compressive out-of-plane strength σ_3 , MPa	–	2.3

Table 6 Wrinkling experiments on glass face/Nomex honeycomb core sandwich specimens and comparison with theories

Sample	Wrinkling load (kN)			
1	17.161			
2	17.006			
3	18.659			
4	17.278			
5	18.644			
6	18.072			
7	17.489			
Average experimental (SD)	Hoff–Mautner	HSAPT	EHSAPT (PFLC)	EHSAPT (USNLC)
17.758 (0.646)	18.57 (4.6%)	15.281 (–13.9%) (S17)	17.158 (–3.4%) (S16)	17.164 (–3.3%) (S16)

A and S in the wave numbers stand for anti-symmetric and symmetric, respectively

the experimental results may be due to the slight waviness of the face sheets that occur during manufacturing process of the sandwich specimens.

In Table 6, the experimental results are compared with the predictions from the various approaches. It should be noted that the theories do not take into account initial imperfections such as waviness of the faces that can occur during manufacturing. Therefore, perfect agreement between experiment and theory is not to

Table 7 Comparison of the theories with the wrinkling experiments of Norris et al. [9]

Face f , in.	Core $2c$, in.	Ratio $2c/f$	Length a , in.	Experimental average σ_{cr} , ksi	Hoff– Mautner σ_{cr} , ksi (% Error)	HSAPT σ_{cr} , ksi (% Error) (n)	EHSAPT (PFLC) σ_{cr} , ksi (% Error) (n)	EHSAPT (USNLC) σ_{cr} , ksi (% Error) (n)
0.0196	1	51.0	3.63	9.817	5.986 (−39.0%)	8.264 (−15.8%) (S4)	8.51 (−13.3%) (A2)	8.491 (−13.5%) (A2)
0.0120	0.75	62.5	2.87	10.422	5.986 (−42.6%)	7.452 (−28.5%) (S5)	9.19 (−11.8%) (A4)	9.175 (−12.0%) (A4)
0.0120	1	83.3	3.85	10.418	5.986 (−42.5%)	6.492 (−37.7%) (S6)	9.61 (−7.8%) (A6)	9.597 (−7.9%) (A6)

Aluminum face/granulated-cork core

be expected. Yet, both EHSAPT approaches are remarkably close to the experimental data and provide the most accurate predictions compared with all other available approaches. In particular, the Hoff–Mautner's conservative formula predicts a nonconservative critical stress in the face sheets and is within 4.6% error. Both the HSAPT and the EHSAPT predict the wrinkling mode to be symmetric and conservative loads. However, the EHSAPT is closest to experiments (within 3.4% error for both approaches), while the HSAPT is more conservative (underpredicting by about 14%).

6 Comparison with wrinkling tests in the literature

Experimental wrinkling stresses of sandwich panels with 24ST clad aluminum face sheets and granulated-cork core (with 0.35 specific gravity) are reported in Norris et al. [9] for three different geometric core-to-facesheet thickness ratios of $2c/f = \{3.63, 2.87, 3.85\}$. The aluminum face sheets had a modulus $E^f = 10^7$ psi, and the granulated-cork core had the following mechanical properties: $E_1^c = 1.18$ ksi, $E_3^c = 0.52$ ksi, $G_{31}^c = 0.33$ ksi and $\nu_{31}^c = 0.06$. The width of all the specimens were 2 in. For a given sandwich configuration, only specimens that had the same exact lengths were considered for comparison. Only 3 specimens had a length of 3.63 in for the $2c/f$ ratio of 3.63, while there were 5 specimens each for configurations with $2c/f$ of 2.87 and 3.85. This set of experimental data was chosen for comparison because it is known that wrinkling was the cause of failure and the tests had good repeatability; the standard deviation is no greater than 0.78 ksi for all 3 configurations.

Table 7 shows the average wrinkling stress in the faces from the experiments as well as those predicted from Hoff–Mautner, HSAPT, and EHSAPT (both PFLC and USNLC methods). The Hoff–Mautner is very conservative (generally about 40% lower) and is the same for the three configurations because the formula is independent of the geometry. The EHSAPT is in best agreement with the experimental data, staying within 14% of the experimental results for the three configurations and is always conservative. Moreover, both EHSAPT approaches are close to each other for all three configurations. The HSAPT is less accurate, being as much as 38% below the experimental data and becomes less accurate as the ratio of $2c/f$ increases. The predicted mode of the high-order theories are also shown in parenthesis. S and A stand for symmetric and antisymmetric, respectively, and is followed by the semi-wave number. The HSAPT predicts symmetric wrinkling mode, unlike the EHSAPT, which predicts antisymmetric wrinkling.

7 Conclusions

The wrinkling formulation based on the EHSAPT was presented. Two different solution procedures were pursued using the EHSAPT: Case (a), in which the compressive loading is applied on the faces and the core strains are assumed linear (PFLC) and Case (b), in which a uniform compressive strain through the thickness is applied and the core strains are assumed nonlinear (USNLC).

The wrinkling predictions of the EHSAPT, the earlier HSAPT, and the Hoff–Mautner's semi-empirical formula are compared with (a) predictions from elasticity and (b) wrinkling experiments. Two experimental sets are chosen for comparison: one set is experiments conducted by the authors on Glass face/Nomex

Honeycomb core sandwich specimens and the other set is experiments from the literature on Aluminum faces/granulated-cork core system.

In all cases, the EHSAPT was the closest to both the elasticity predictions and the experimental data. There was little difference between the two formulations of the EHSAPT, which argues for the much simpler PFLC (loading on faces, linear core) approach. The earlier HSAPT was in significant error for the relatively thinner faces. The large discrepancy between HSAPT and EHSAPT for very low f/h_{tot} (when the beam is most susceptible to wrinkling), and the associated smaller discrepancy for higher f/h_{tot} (when the beam tends to buckle globally), indicates that including the axial rigidity of the core is very important during wrinkling.

The comparison of the different wrinkling formulations with elasticity shows that in general the semi-empirical Hoff–Mautner formula is quite conservative, yet less so than the HSAPT. The good agreement of the EHSAPT with the experiments on honeycomb core sandwich specimens shows that although the EHSAPT models the core as a homogenous material with global properties, the theory can be used to predict critical loads of nonhomogeneous honeycomb cores just as well as for homogeneous solid cores.

Acknowledgments The financial support of the Office of Naval Research, Grant N00014-07-10373, and the interest and encouragement of the Grant Monitor, Dr. Y. D. S. Rajapakse, are both gratefully acknowledged.

Appendix A: Elements of the $[K_{LC}]$ matrix

The $[K_{LC}]$ matrix is 7×7 symmetric matrix and has the following elements, k_{ij} , $i, j = 1, \dots, 7$:

$$k_{11} = \frac{47}{30c}C_{55}^c + \frac{6c\alpha_n^2}{35}C_{11}^c + C_{11}^b f_b \alpha_n^2; \quad k_{12} = -\frac{4}{3c}C_{55}^c + \frac{2c\alpha_n^2}{15}C_{11}^c, \quad (\text{A1a})$$

$$k_{13} = \frac{4}{5}C_{55}^c - \frac{2c^2\alpha_n^2}{35}C_{11}^c; \quad k_{14} = -\frac{7}{30c}C_{55}^c + \frac{c\alpha_n^2}{35}C_{11}^c, \quad (\text{A1b})$$

$$k_{15} = -\frac{3cf_b\alpha_n^3}{35}C_{11}^c - \eta_3^b\alpha_n; \quad k_{16} = -\alpha_n\beta_1; \quad k_{17} = \frac{cf_t\alpha_n^3}{70}C_{11}^c + \eta_2^t\alpha_n. \quad (\text{A1c})$$

$$k_{22} = \frac{8}{3c}C_{55}^c + \frac{16c\alpha_n^2}{15}C_{11}^c; \quad k_{23} = 0; \quad k_{24} = k_{12}, \quad (\text{A2a})$$

$$k_{25} = -\frac{cf_b\alpha_n^3}{15}C_{11}^c + \eta_6^b\alpha_n; \quad k_{26} = 0; \quad k_{27} = \frac{cf_t\alpha_n^3}{15}C_{11}^c - \eta_6^t\alpha_n. \quad (\text{A2b})$$

$$k_{33} = \frac{8c}{5}C_{55}^c + \frac{16c^3\alpha_n^2}{105}C_{11}^c; \quad k_{34} = -\frac{4}{5}C_{55}^c + \frac{2c^2\alpha_n^2}{35}C_{11}^c, \quad (\text{A3a})$$

$$k_{35} = \frac{c^2f_b\alpha_n^3}{35}C_{11}^c - \eta_4^b\alpha_n; \quad k_{36} = \frac{4c\beta_1\alpha_n}{3}; \quad k_{37} = \frac{c^2f_t\alpha_n^3}{35}C_{11}^c - \eta_4^t\alpha_n. \quad (\text{A3b})$$

$$k_{44} = \frac{47}{30c}C_{55}^c + \frac{6c\alpha_n^2}{35}C_{11}^c + C_{11}^t f_t \alpha_n^2; \quad k_{45} = -\frac{cf_b\alpha_n^3}{70}C_{11}^c - \eta_2^b\alpha_n, \quad (\text{A4a})$$

$$k_{46} = \beta_1\alpha_n; \quad k_{47} = \frac{3cf_t\alpha_n^3}{35}C_{11}^c + \eta_3^t\alpha_n. \quad (\text{A4b})$$

$$k_{55} = \frac{7}{6c}C_{33}^c + \frac{3cf_b^2\alpha_n^4}{70}C_{11}^c + \frac{f_b^3\alpha_n^4}{12}C_{11}^b - \eta_8^b\alpha_n^2; \quad k_{56} = -\frac{4}{3c}C_{33}^c - \eta_7^b\alpha_n^2, \quad (\text{A5a})$$

$$k_{57} = \frac{1}{6c}C_{33}^c - \frac{cf_b f_t \alpha_n^4}{140}C_{11}^c - \beta_2\alpha_n^2. \quad (\text{A5b})$$

$$k_{66} = \frac{8}{3c}C_{33}^c + \frac{16c\alpha_n^2}{15}C_{55}^c; \quad k_{67} = -\frac{4}{3c}C_{33}^c - \eta_7^t\alpha_n^2. \quad (\text{A6})$$

$$k_{77} = \frac{7}{6c}C_{33}^c + \frac{3cf_t^2\alpha_n^4}{70}C_{11}^c + \frac{f_t^3\alpha_n^4}{12}C_{11}^t - \eta_8^t\alpha_n^2. \quad (\text{A7})$$

where

$$\alpha_n = \frac{n\pi}{a}, \quad \eta_2^i = \frac{1}{30}C_{13}^c + \left(\frac{1}{30} - \frac{7f_i}{60c}\right)C_{55}^c, \quad (\text{A8a})$$

$$\eta_3^i = -\frac{11}{30}C_{13}^c + \left(\frac{19}{30} + \frac{47f_i}{60c}\right)C_{55}^c, \quad \eta_4^i = \frac{4c}{15}C_{13}^c + \left(\frac{4c}{15} + \frac{2f_i}{5}\right)C_{55}^c, \quad (\text{A8b})$$

$$\eta_6^i = \frac{2}{3}C_{13}^c + \left(\frac{2}{3} + \frac{2f_i}{3c}\right)C_{55}^c, \quad \eta_7^i = -\frac{f_i}{5}C_{13}^c - \left(\frac{2c}{15} + \frac{f_i}{5}\right)C_{55}^c \quad (\text{A8c})$$

$$\eta_8^i = \frac{11f_i}{30}C_{13}^c - \left(\frac{4c}{15} + \frac{19f_i}{30} + \frac{47f_i^2}{120c}\right)C_{55}^c, \quad \eta_{4a}^i = \eta_4^i - \left(\frac{2c}{3} + f_i\right)C_{55}^c \quad (\text{A8d})$$

$$\eta_{6a}^i = C_{13}^c - \eta_6^i, \quad \eta_{7a}^i = \frac{2c + 3f_i}{6}C_{55}^c + \eta_7^i$$

$$\eta_{8a}^i = \frac{11f_i}{60}C_{13}^c - \eta_8^i, \quad (\text{A8e})$$

and

$$\beta_1 = \frac{2}{5}(C_{13}^c + C_{55}^c), \quad (\text{A9a})$$

$$\beta_2 = \frac{f_b + f_t}{60}C_{13}^c + \left(\frac{c}{15} + \frac{f_b + f_t}{60} - \frac{7f_b f_t}{120c}\right)C_{55}^c, \quad (\text{A9b})$$

References

1. Carlsson, L.A., Kardomateas, G.A.: Structural and Failure Mechanics of Sandwich Composites, Chapter 8. Springer, Dordrecht (2011)
2. Hoff, N.J., Mautner, S.F.: The buckling of Sandwich-type panels. *J. Aeronaut. Sci.* **12**(3), 285–297 (1945)
3. Allen, H.G.: Analysis and Design of Structural Sandwich Panels, Chapter 8. Pergamon Press, Oxford (1969)
4. Frostig, Y., Baruch, M., Vilnay, O., Sheinman, I.: High-order theory for Sandwich-beam behavior with transversely flexible core. *J. Eng. Mech.* **118**(5), 1026–1043 (1992)
5. Phan, C.N., Frostig, Y., Kardomateas, G.A.: Analysis of Sandwich panels with a compliant core and with in-plane rigidity-extended high-order Sandwich panel theory versus elasticity. *J. Appl. Mech. (ASME)* **79**, 041001 (2012)
6. Vonach, W.K., Rammerstorfer, F.G.: The effect of in-plane core stiffness on the wrinkling behavior of thick Sandwiches. *Acta Mech.* **141**, 1–10 (2000)
7. Kardomateas, G.A.: Wrinkling of wide Sandwich panels/beams with orthotropic phases by an elasticity approach. *J. Appl. Mech. (ASME)* **72**, 818–825 (2005)
8. Ley, R.P., Weichuan, L., Mbanefo, U.: Facesheet Wrinkling in Sandwich Structures. NASA/CR-1999-208994 (1999)
9. Norris, C.B., Wilhelm, E.S., March, H.W., Smith, C.B., Boller, K.H.: Wrinkling of the Facings of Sandwich Construction Subjected to Edgewise Compression, FPL Report No. 1810 (1961)
10. Phan, C.N., Kardomateas, G.A., Frostig, Y.: Global Buckling of a Sandwich Wide Panel/Beam Based on the Extended High Order Theory. *AIAA. J.* (in press) (2012)
11. Frostig, Y., Baruch, M.: High-order buckling analysis of Sandwich beams with transversely flexible core. *J. Eng. Mech.* **119**(3), 476–495 (1993)
12. Goodier, J.N., Neou, I.M.: The evaluation of theoretical compression in Sandwich plates. *J. Aeronaut. Sci.* **18**(10), 649–657 (1951)